Microscopic description of complex nuclear decay: multimodal fission

A. Staszczak,[1,2,3] A. Baran,[1,2,3] J. Dobaczewski,[4,5] and W. Nazarewicz[2,3,4]

[1]*Institute of Physics, Maria Curie-Skłodowska University, pl. M. Curie-Skłodowskiej 1, 20-031 Lublin, Poland*
[2]*Department of Physics and Astronomy, University of Tennessee Knoxville, TN 37996*
[3]*Physics Division, Oak Ridge National Laboratory, P.O. Box 2008, Oak Ridge, TN 37831*
[4]*Institute of Theoretical Physics, University of Warsaw, ul. Hoża 69, 00-681 Warsaw, Poland*
[5]*Department of Physics, P.O. Box 35 (YFL), FI-40014 University of Jyväskylä, Finland*

(Dated: June 23, 2009)

Our understanding of nuclear fission, a fundamental nuclear decay, is still incomplete due to the complexity of the process. In this paper, we describe a study of spontaneous fission using the symmetry-unrestricted nuclear density functional theory. Our results show that the observed bimodal fission can be explained in terms of pathways in multidimensional collective space corresponding to different geometries of fission products. We also predict a new phenomenon of trimodal spontaneous fission for some rutherfordium, seaborgium, and hassium isotopes.

PACS numbers: 21.60.Jz, 24.75.+i, 27.90.+b

I. INTRODUCTION

Seventy years ago Joliot Curie and Savitch [1] discovered that the exposure of uranium to neutrons leads to the existence of lanthanum. Following this finding, Hahn and Strassmann [2] proved definitively that bombarding uranium with neutrons produces alkali earth elements, ushering in what has come to be known as the atomic age. The term nuclear fission was coined one year later by Meitner and Frisch [3], who explained experimental results in terms of the division of a heavy nucleus into two lighter nuclei. In 1939, Bohr and Wheeler [4] developed a theory of fission based on a liquid drop model. Interestingly, their work also contained an estimate of a lifetime for fission in the ground state. Soon afterwards, Petrzhak and Flerov [5] presented the first experimental evidence for such spontaneous fission (SF).

While early descriptions of fission were based on a purely geometrical framework of the nuclear liquid drop model [4] (i.e., shape-dependent competition between Coulomb and surface energy), it was soon realized [6] that the single-particle motion of protons and neutrons moving in a self-deforming mean field is crucial for the understanding of a range of phenomena such as fission half-lives, mass and energy distributions of yields, cross sections, and fission isomers [7, 8]. In the macroscopic-microscopic method (MMM) proposed by Swiatecki [9] and Strutinsky *et al.* [10, 11], quantum shell effects are added atop the average (or macroscopic) behavior described by the liquid drop, and this approach turned out to be very successful in explaining many features of SF [12, 13, 14].

Quantum mechanically, fission represents a time-dependent solution of the many-body Schrödinger equation where all particles move collectively. To fully solve such a time-dependent problem for more than 200 particles is neither possible nor sensible because the essence of the process is in its coherence. Consequently, most of the essential physics should be contained in underlying mean fields. This determines the choice of a microscopic tool to be used: the nuclear density functional theory (DFT) [15]. The advantage of DFT is that, while treating the nucleus as a many-body system of fermions, it provides an avenue for identifying the essential collective degrees of freedom.

Because the commonly used nuclear density functionals are usually adjusted to nuclear ground-state properties and infinite nuclear matter, and most applications are symmetry-restricted to speed up computations, self-consistent theories typically are not as quantitative as MMM when it comes to SF, except for some cases [16]. It is only recently that an effort has been made to systematically optimize the effective forces by considering experimental data relevant to large deformations [17].

In this work, we provide a microscopic description of multi-mode fission based on the symmetry-unrestricted nuclear DFT. Since many observed fission characteristics can be traced back to topologies of fission pathways in multidimensional collective space [12], allowing for arbitrary shapes on the way to fission is the key. To this end, we search for the optimum collective trajectory in a multidimensional space. The barrier penetration probability, or a fission half-life, is computed by integrating the action along this optimum path. In practice, this is done by constraining the nuclear collective coordinates associated with shape deformations to have prescribed values of the lowest multipole moments, $Q_{\lambda\mu}$ by which we explore the main degrees of freedom related to elongation ($\lambda\mu = 20$), reflection-asymmetry ($\lambda\mu = 30$), and necking ($\lambda\mu = 40$). The effects due to triaxiality are known to be important around the top of the first fission barrier [13, 18, 19, 20, 21, 22]. Indeed, the first saddle point is lowered by several MeV by triaxial degrees of freedom. In our work, we take into account the impact of non-axial degrees of freedom by considering the triaxial quadrupole moment ($\lambda\mu = 22$).

The paper is organized as follows. Section II describes the details of our model. The results of calculations are

discussed in Sec. III. Finally, Sec. IV summarizes the main results of our study and offer perspectives for future work.

II. THE MODEL

The calculations were carried out using a symmetry-unrestricted DFT program based on the Hartree Fock-Bogoliubov solver HFODD [23, 24] capable of treating simultaneously all the possible collective degrees of freedom that might appear on the way to fission. Based on this DFT framework, we calculated the total energy along the fission pathways, corresponding collective inertia (collective masses) and zero point energy (ZPE) corrections to account for quantum fluctuations.

In the particle-hole channel, we use the SkM* energy density functional [25] that has been optimized at large deformations; hence it is often used for fission barrier predictions. In the pairing channel, we adopted a seniority pairing force with the strength parameters fitted to reproduce the experimental gaps in ^{252}Fm [26]. Because the nuclei considered are all well bound, pairing could be treated within the BCS approximation. The single-particle basis consisted of the lowest 1,140 stretched states originating from the lowest 31 major oscillator shells.

In the analysis of fission pathways, we explored multidimensional collective space. To separate fission pathways, we computed energy surfaces in the deformation spaces $\{Q_{20}, Q_{30}\}$ and $\{Q_{20}, Q_{40}\}$. The calculations were not limited to axial shapes; triaxial deformations appear if energetically favorable (e.g., within the inner barrier). At each deformation point, defined by the set of constrained multipole moments, fully self-consistent DFT equations have been solved, whereupon the total energy of the system is always minimized with respect to all remaining (i.e., unconstrained) shape parameters. The optimum 1D paths have been localized in the form of multipole moments, Q_{30}, Q_{22}, and Q_{40}, becoming functions of the driving moment, Q_{20}.

The vibrational and rotational ZPE corrections and the cranking quadrupole mass parameter were calculated as described in Ref. [27]. The spontaneous fission half-lives were estimated from the WKB expression for the double-humped potential barrier [28, 29] assuming a 1D tunneling path along Q_{20}.

III. RESULTS

To demonstrate the validity and generality of our method, we chose a case where several fission pathways were known to coexist and all intrinsic symmetries of the nuclear mean field were broken. In this respect, a phenomenon known as bimodal fission, observed in several fermium and transfermium nuclei [30, 31, 32, 33], is a perfect testing ground. It manifests itself, for example, in a sharp transition from an asymmetric mass division in ^{256}Fm and ^{256}No to a symmetric mass split in ^{258}Fm and ^{258}No. Furthermore, the total kinetic energy distributions of the fission fragments appear to have two peaks centered around 200 and 233 MeV. It has been suggested [32, 34, 35, 36, 37, 38] that the higher energy fission mode corresponds to a scission configuration associated with two touching, nearly spherical, fragments with the maximal Coulomb repulsion, whereas the lower-energy mode can be associated with more elongated fragments. Before this work, bimodal fission was studied within the MMM [13, 34, 35, 36, 37] and nuclear DFT [19, 22, 39, 40, 41, 42]. All those studies were symmetry-restricted (i.e., they did not consider simultaneous inclusion of elongation, triaxiality, and reflection-asymmetry).

A. Fission pathways of the fermium isotopes

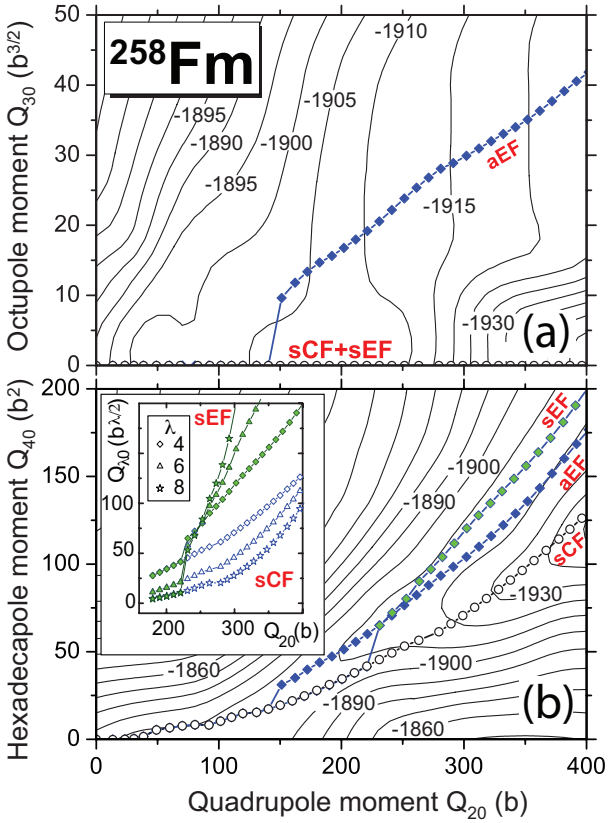

FIG. 1: (Color online) Two-dimensional total energy surfaces for ^{258}Fm in the plane of collective coordinates: Q_{20}-Q_{30} (a), and Q_{20}-Q_{40} (b). The fission pathways are marked: symmetric compact fragments (sCF), symmetric elongated fragment (sEF), and asymmetric elongated fragments (aEF) pathways. The difference between contour lines is 5 MeV in (a) and 10 MeV in (b). The asymmetric trajectory aEF bifurcates away near $Q_{20} \approx 150$ b from Q_{30}=0 while the bifurcation between sEF and sCF occurs near $Q_{20} \approx 225$ b. The inset shows the multipole moments $Q_{\lambda 0}$ along sCF and sEF.

To identify saddle points and fission pathways in a multidimensional energy surface is not a simple task. As pointed out in earlier studies [12, 13, 43, 44], saddle points obtained in calculations constrained by only one collective variable are sometimes incorrect; hence, special numerical techniques are required to find them. To this end, we computed two-dimensional (2D) energy surfaces in $\{Q_{20}, Q_{30}\}$ and $\{Q_{20}, Q_{40}\}$ planes. Based on the initial 2D uniform grids, Q_{20}=0(10)400 b, Q_{30}=0(5)50 b$^{3/2}$, and Q_{40}=0(10)200 b^2, we calculated the constrained HF+BCS energy. In our HFODD calculations we employed the standard method of quadratic constraint (the quadratic penalty method) [45, 46]. Within this approach, the moments calculated from the converged densities differ slightly from the requested values defining the constraints [46]. This implies that the final mesh used for interpolation is non-uniform. Using the self-consistent values of multipole moments, the non-uniform interpolation was carried out to produce the final result. Figure 1 shows 2D energy surfaces for ^{258}Fm.

The 1D fission pathways shown in Fig. 1 were obtained by finding the local energy minimum at a given value of Q_{20} and following this solution when gradually increasing the driving moment Q_{20}. This method thus relies on local properties of the Q_{20}-constrained energy surface. In practice, one obtains different energy surfaces locally valid around each fission pathway. In order to facilitate the presentation, however, we carried out interpolation between different energy sheets. For that reason, the contour lines in Fig. 1 slightly depend on the algorithm used to interpolate between 2D constrained results; hence, the 2D surfaces should be considered as a qualitative guidance on the topological structure of the energy surface.

Beyond the first barrier, at $Q_{20} \approx 150$ b, a reflection-asymmetric path corresponding to asymmetric elongated fragments (aEFs) branches away from the symmetric valley, see Fig. 1a. At $Q_{20} \simeq 225$ b, a reflection-symmetric path splits into two branches: one corresponding to nearly spherical symmetric compact fragments (sCFs) and one associated with symmetric elongated fragments (sEFs). This bifurcation is clearly seen in Fig. 1b. Such three fission pathways were predicted in early work based on MMM [34, 36] and also found recently within a DFT framework [40, 41], except that the axial-symmetry was enforced in all these studies.

A pattern of similarly competing fission valleys was found for all investigated isotopes. As an illustrative example, the results of our 1D fission pathway calculations for ^{252,258,264}Fm are displayed in Fig. 2. (The energy curves corresponding to individual pathways in ^{256,260}Fm can be found in our earlier work [26].) The transition from an asymmetric fission path in ^{252}Fm to a compact-symmetric path in ^{264}Fm is due to shell effects in the emerging fission fragments approaching the doubly magic nucleus ^{132}Sn [32, 35, 47, 48, 49]. The triaxial deformations are important around the first (inner) fission barrier, and they reduce the fission barrier height by several MeV.

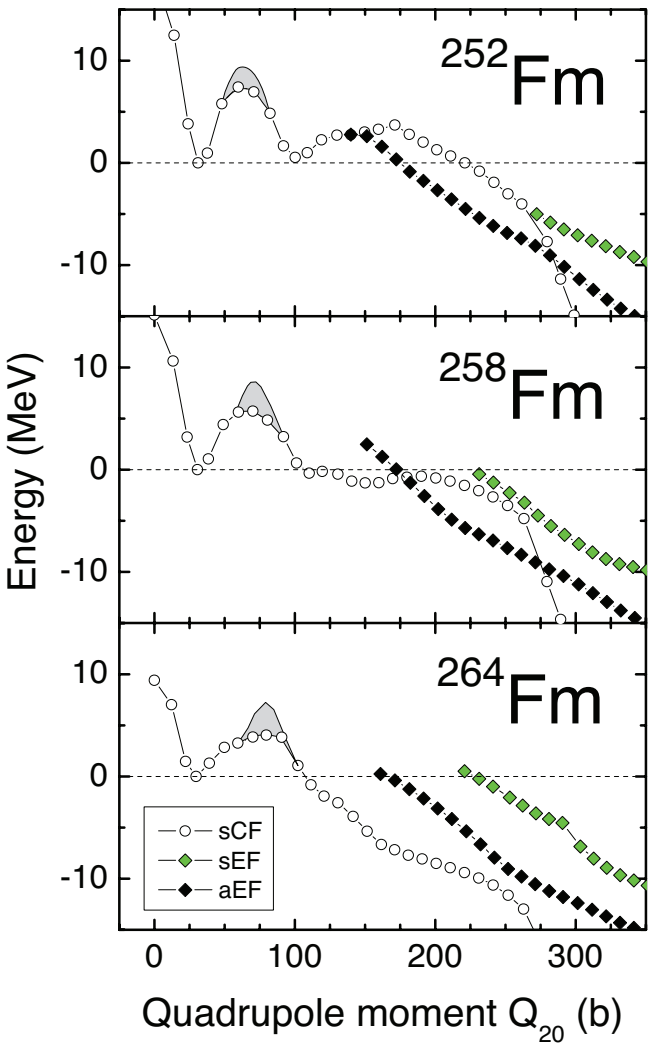

FIG. 2: (Color online) Calculated 1D fission pathways for ^{252,258,264}Fm as functions of the driving quadrupole moment, Q_{20}. Open circles, light diamonds, and dark diamonds denote the symmetric compact fragment (sCF), symmetric elongated fragment (sEF), and asymmetric elongated fragment (aEF) valleys, respectively. The effect of triaxiality is important in the region of the first barrier; the corresponding energy gain is marked by gray shading.

While the asymmetric pathway aEF is favored in the lighter Fm isotopes, e.g., ^{252}Fm, both symmetric paths are open for ^{258}Fm, due to the disappearance of the outer fission barrier in sCF and sEF. It is to be noted that the symmetric pathways sCF and sEF in ^{258}Fm are predicted to bifurcate away well outside the first barrier (see also recent work [50] based on MMM).

In the case of $^{260-264}$Fm, we find that there is no outer potential barrier along the sCF trajectory, and the sEF and aEF paths lie significantly higher in the outer region. It should be emphasized that the pathways correspond to different regions of the collective space and this is apparent when studying them in more than one dimension. Indeed, aEF is well separated from sCF and sEF in Q_{30}

(the apparent crossing between aEF and sEF in Fig. 1b is an artifact of the 2D projection) while the symmetric trajectories sCF and sEF strongly differ in the values of higher multipole moments λ=4, 6, and 8 (see the inset in Fig. 1).

B. Spontaneous fission half-lives

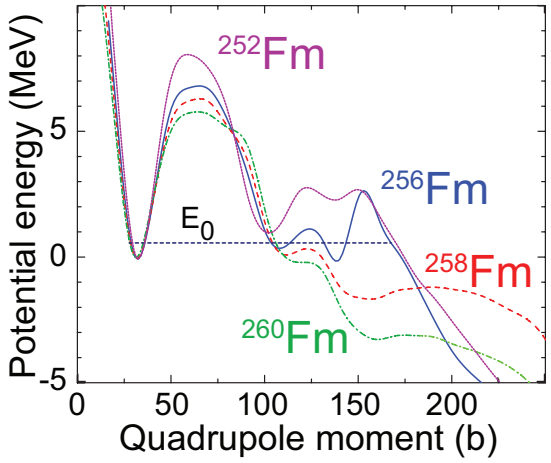

FIG. 3: (Color online) Potential energy curves of ^{252}Fm, ^{256}Fm, ^{258}Fm, and ^{260}Fm along optimum 1D paths containing the quantum zero-point energy correction, drawn in the common scale relative to values calculated at the ground-state minima.

Having determined the lowest fission valleys, i.e., the lowest energy pathways along Q_{20}, we computed the corresponding ZPE corrections. The resulting collective potentials are plotted in Fig. 3 for ^{252}Fm, ^{256}Fm, ^{258}Fm, and ^{260}Fm. It is seen that when going from ^{252}Fm to ^{260}Fm, the first barrier gets reduced and the outer barrier disappears altogether.

To assess the SF half-lives theoretically, we calculated the collective inertia parameter along Q_{20} and performed WKB barrier penetration calculations for even-even fermium isotopes with 242≤A≤260. We assumed two values of the ground state energy counted from the ground state potential energy minimum: E_0=0.3 MeV and the commonly used value [51] of 0.5 MeV. The resulting SF half-lives are shown in Fig. 4. In spite of a fairly simple 1D penetration picture, it is satisfying to see a quantitative agreement between experiment [52, 53] and theory (for Gogny-DFT results, see [40]). The existence of a small outer barrier in ^{256}Fm is significant as it increases the fission half-life in this nucleus by more than four orders of magnitude compared to that of ^{258}Fm, thus explaining the rapid change in experimental SF half-lives between these nuclei.

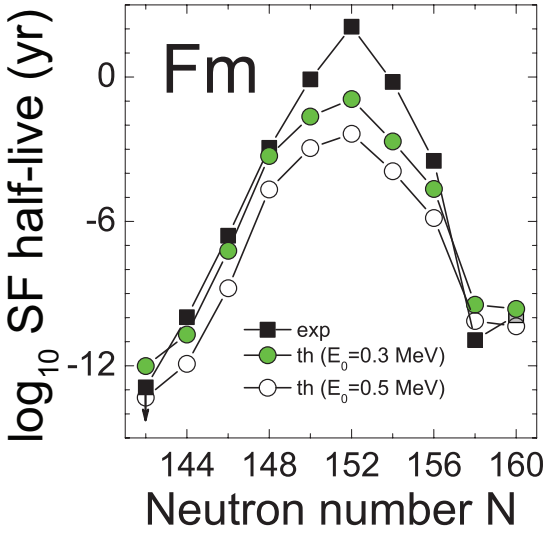

FIG. 4: (Color online) Fission half lives of even-even fermium isotopes with 242≤A≤260, calculated in this study compared with experimental data [52, 53] for the two values of the zero-point energy E_0=0.3 MeV and 0.5 MeV.

C. Multimodal fission

To map out the competition between different fission pathways in the heaviest elements, we carried out systematic calculations for even-even nuclei with 98≤Z≤108 and 154≤N≤160. A transition from the usual asymmetric fission channel seen in the actinides to compact symmetric fission is seen when moving towards ^{264}Fm. In the intermediate region of bimodal fission, two symmetric channels coexist. Around ^{260}Sg (Z=106, N=154), our calculations predict trimodal fission, i.e., competition between the asymmetric fission valley and two symmetric ones. (The term "multimodal fission" has been previously used by M.G. Itkis *et al.* [54] in the context of fusion-fission and quasi-fission of hot superheavy nuclei produced in heavy ion reactions.)

The representative fission pathways for ^{254}Cf (asymmetric fission), ^{260}Fm (symmetric compact fission), ^{258}No (bimodal fission) and ^{262}Hs (trimodal fission) are displayed in Fig. 5. The inclusion of triaxiality significantly reduces the inner barrier in ^{254}Cf, ^{260}Fm, and ^{258}No while the effect in ^{262}Hs is much weaker. Other nuclei from this region exhibit similar pattern of fission pathway competition. A summary of our findings is given in Fig. 6.

IV. SUMMARY

In summary, the symmetry-unrestricted nuclear DFT framework has been applied to the problem of SF. As an example, we studied the challenging case of static SF pathways in ^{256}Fm, ^{258}Fm, and ^{260}Fm and in a number of neighboring nuclei. We found competition

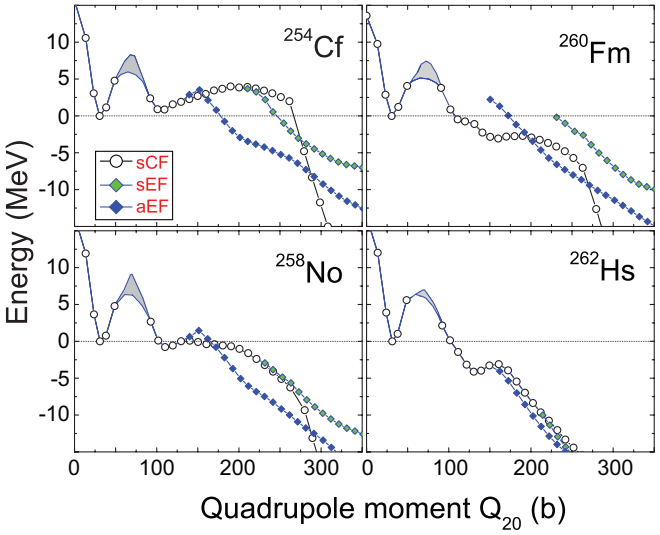

FIG. 5: (Color online) Similar as in Fig. 2 except for fission pathways in ^{254}Cf (asymmetric fission), ^{260}Fm (symmetric compact fission), ^{258}No (bimodal fission) and ^{262}Hs (trimodal fission).

between symmetric-compact, symmetric-elongated, and asymmetric-elongated fission valleys that is consistent with the observed distribution of fission yields. The saddle points obtained in constrained 1D calculations were confirmed through an analysis of 2D energy surfaces. From the calculated collective potential and collective mass, we estimated SF half-lives, and good agreement with experimental data was found. Finally, we predicted trimodal fission for several rutherfordium, seaborgium, and hassium isotopes.

It is worth noting that calculations of self-consistent energy 2D surfaces are computer intensive. Because a single HFODD run with all self-consistent symmetries broken takes about 60 minutes of CPU time, it takes about 3 CPU-years to carry out the full fission pathway analysis for 24 nuclei; hence, massively parallel computer platforms had to be used.

In the near term, we intend to improve the theory of SF half-lives by considering multidimensional inertia tensors and by performing the direct minimization of the collective action in a multidimensional collective space [55]. In the long term, the theory will be extended to account for nonadiabatic effects (e.g., along the lines of Refs. [56, 57]). In addition, quality microscopic input for fission calculations is needed. Of particular importance is the development of the nuclear energy density functional better reproducing both bulk nuclear properties and spectroscopic data.

This work was supported in part by the National Nuclear Security Administration under the Stewardship Science Academic Alliances program through U.S. Department of Energy Research Grant DE-FG03-03NA00083; by the U.S. Department of Energy under Contract Nos. DE-FG02-96ER40963 (University of Tennessee), DE-

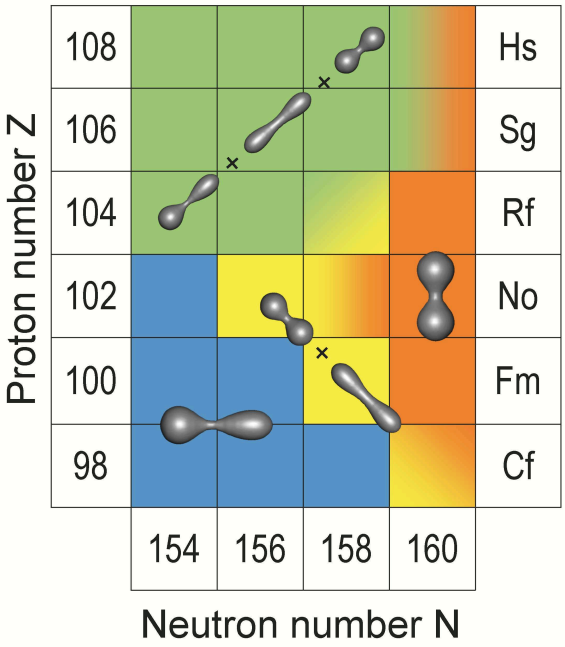

FIG. 6: (Color online) Summary of fission pathway results obtained in the present study. Nuclei around ^{252}Cf$_{154}$ are predicted to fission along the asymmetric path aEF; those around ^{262}No$_{160}$ along the symmetric pathway sCF. These two regions are separated by the bimodal symmetric fission (sCF + sEF) around ^{258}Fm$_{158}$. In a number of the Rf, Sg, and Hs nuclei, all three fission modes are likely (aEF + sCF + sEF; trimodal fission). In some cases, labelled by two-tone shading with one tone dominant, calculations predict coexistence of two decay scenarios with a preference for one. Typical nuclear shapes corresponding to the calculated nucleon densities are marked.

AC05-00OR22725 with UT-Battelle, LLC (Oak Ridge National Laboratory), and DE-FC02-09ER41583 (UNEDF SciDAC Collaboration); by the Polish Ministry of Science and Higher Education under Contract No. N N 202 328234; and by the Academy of Finland and University of Jyväskylä within the FIDIPRO program. Computational resources were provided by the National Center for Computational Sciences at Oak Ridge National Laboratory.

[1] I. Curie and P. Savitch, J. Phys. Rad. **9**, 355 (1938).
[2] O. Hahn and F. Strassmann, Naturwissenschaften **27**, 11 (1939).
[3] L. Meitner and O.R. Frisch, Nature **143**, 239 (1939).
[4] N. Bohr and J.A. Wheeler, Phys. Rev. **56**, 426 (1939).
[5] K.A. Petrzhak and G.N. Flerov, J. Phys. USSR **3**, 275

(1940); Phys. Rev. **58**, 89 (1940).
[6] D.L. Hill and J.A. Wheeler, Phys. Rev. **89**, 1102 (1953).
[7] C. Wagemans, *The Nuclear Fission Process* (CRC Press, Boca Raton, Florida, 1991).
[8] S. Bjørnholm and J.E. Lynn, Rev. Mod. Phys. **52** (1980) 725.
[9] W.J. Swiatecki, Phys. Rev. **100**, 937 (1955).
[10] V.M. Strutinsky, Nucl. Phys. A **95**, 420 (1967).
[11] M. Brack, J. Damgård, A.S. Jensen, H.C. Pauli, V.M. Strutinsky, and C.Y. Wong, Rev. Mod. Phys. **44**, 320 (1972).
[12] P. Möller, D.G. Madland, A.J. Sierk, and A. Iwamoto, Nature **409**, 785 (2001).
[13] P. Möller, A.J. Sierk, T. Ichikawa, A. Iwamoto, R. Bengtsson, H. Uhrenholt, and S. Åberg, Phys. Rev. C **79**, 064304 (2009).
[14] A. Sobiczewski and K. Pomorski, Prog. Part. Nucl. Phys. **58**, 292 (2007).
[15] M. Bender, P.-H. Heenen, and P.-G. Reinhard, Rev. Mod. Phys. **75**, 121 (2003).
[16] H. Goutte, J.F. Berger, P. Casoli, and D. Gogny, Phys. Rev. C **71**, 024316 (2005).
[17] S. Goriely, M. Samyn, and J.M. Pearson, Phys. Rev. C **75**, 064312 (2007).
[18] S.E. Larsson, I. Ragnarsson, and S.G. Nilsson, Phys. Lett. B **38** (1972) 269.
[19] M. Bender, K. Rutz, P.-G. Reinhard, J.A. Maruhn, and W. Greiner, Phys. Rev. C **58**, 2126 (1998).
[20] T. Bürvenich, M. Bender, J.A. Maruhn, and P.-G. Reinhard, Phys. Rev. C **69**, 014307 (2004); Erratum-ibid. C **69**, 029901 (2004).
[21] A. Staszczak, J. Dobaczewski, and W. Nazarewicz, AIP Conference Proceedings **798**, 93 (2005).
[22] J.P. Delaroche, M. Girod, H. Goutte, and J. Libert, Nucl. Phys. A **771**, 103 (2006).
[23] J. Dobaczewski and P. Olbratowski, Comput. Phys. Commun. **158**, 158 (2004); *ibid.* **167**, 214 (2005).
[24] J. Dobaczewski, W. Satuła, B.G. Carlsson, J. Engel, P. Olbratowski, P. Powałowski, M. Sadziak, J. Sarich, N. Schunck, A. Staszczak, M.V. Stoitsov, M. Zalewski, and H. Zduńczuk, submitted to Comput. Phys. Commun., arXiv:0903.1020.
[25] J. Bartel, P. Quentin, M. Brack, C. Guet, and H.B. Håkansson, Nucl. Phys. A **386**, 79 (1982).
[26] A. Staszczak, J. Dobaczewski, and W. Nazarewicz, Acta Phys. Pol. B **38**, 1589 (2007).
[27] A. Baran, A. Staszczak, J. Dobaczewski, and W. Nazarewicz, Int. J. Mod. Phys. E **16**, 443 (2007).
[28] A.V. Ignatiuk, N.S. Rabotnov, and G.N. Smirenkin, Phys. Lett. B **29**, 209 (1969).
[29] J.D. Cramer and J.R. Nix, Phys. Rev. C **2**, 1048 (1970).
[30] H.C. Britt, D.C. Hoffman, J. van der Plicht, J.B. Wilhelmy, E. Cheifetz, R.J. Dupzyk, and R.W. Lougheed, Phys. Rev. C **30**, 559 (1984).
[31] E.K. Hulet, J.F. Wild, R.J. Dougan, R.W. Lougheed, J.H. Landrum, A.D. Dougan, M. Schädel, R.L. Hahn, P.A. Baisden, C.M. Henderson, R.J. Dupzyk, K. Sümmerer, and G.R. Bethune, Phys. Rev. Lett. **56**, 313 (1986).
[32] E.K. Hulet, J.F. Wild, R.J. Dougan, R.W. Lougheed, J.H. Landrum, A.D. Dougan, P.A. Baisden, C.M. Henderson, R.J. Dupzyk, R.L. Hahn, M. Schädel, K. Sümmerer, and G.R. Bethune, Phys. Rev. C **40**, 770 (1989).
[33] D.C. Hoffman and M. R. Lane, Radiochimica Acta **70/71**, 135 (1995).
[34] U. Brosa, S. Grossmann, and A. Müller, Z. Phys. A **325**, 241 (1986); Z. Nat. **41a**, 1341 (1986).
[35] P. Möller, J.R. Nix, and W.J. Swiatecki, Nucl. Phys. A **469**, 1 (1987); *ibid.* **492**, 349 (1989).
[36] V.V. Pashkevich, Nucl. Phys. A **477**, 1 (1988).
[37] S. Ćwiok, P. Rozmej, A. Sobiczewski, and Z. Patyk, Nucl. Phys. A **491**, 281 (1989).
[38] Y.L. Zhao, Y. Nagame, I. Nishinaka, K. Sueki, and H. Nakahara, Phys. Rev. C **62**, 014612 (2000).
[39] M. Warda, J.L. Egido, L.M. Robledo, and K. Pomorski, Phys. Rev. C **66**, 014310 (2002).
[40] M. Warda, J.L. Egido, and L M. Robledo, Phys. Scr. **T125**, 226 (2006).
[41] L. Bonneau, Phys. Rev. C **74**, 014301 (2006).
[42] N. Dubray, H. Goutte, and J.-P. Delaroche, Phys. Rev. C **77**, 014310 (2008).
[43] W.D. Myers and W.J. Swiatecki, Nucl. Phys. A **601**, 141 (1996).
[44] A. Mamdouh, J.M. Pearson, M. Rayet, and F. Tondeur, Nucl. Phys. A **644**, 389 (1998).
[45] B. Giraud, J. Le Tourneux, and S.K.M. Wong, Phys. Lett. B **32**, 23 (1970).
[46] H. Flocard, P. Quentin, A.K. Kerman, and D. Vautherin, Nucl. Phys. A **203**, 433 (1973).
[47] D. Poenaru, J.A. Maruhn, W. Greiner, M. Ivascu, D. Mazilu, and R. Gherghescu, Z. Phys. **328**, 309 (1987).
[48] B.S. Bhandari, Phys. Rev. Lett. **66**, 1034 (1991).
[49] F. Gönnenwein, Z. Phys. **349**, 259 (1993); Nucl. Phys. A **654**, 855c (1999).
[50] T. Ichikawa, A. Iwamoto, and P. Möller, Phys. Rev. C **79**, 014305 (2009).
[51] S.G. Nilsson, C.-F. Tsang, A. Sobiczewski, Z. Szymański, S. Wycech, C. Gustafson, I.-L. Lamm, P. Möller, and B. Nilsson, Nucl. Phys. A **131**, 1 (1969).
[52] N.E. Holden and D.C. Hoffman, Pure Appl. Chem. **72**, 1525 (2000).
[53] J. Khuyagbaatar, S. Hofmann, F.P. Hessberger, D. Ackermann, H.G. Burkhard, S. Heinz, B. Kindler, I. Kojouharov, B. Lommel, R. Mann, J. Maurer, K. Nishio, and Yu. Novikov, Eur. Phys. J. A **37**, 177 (2008).
[54] M.G. Itkis, A.A. Bogachev, I.M. Itkis, J. Kliman, G.N. Knyazheva, N.A. Kondratiev, E.M. Kozulin, L. Krupa, Yu.Ts. Oganessian, I.V. Pokrovsky, E.V. Prokhorova, and A.Ya. Rusanov, Nucl. Phys. A **787**, 150c (2007).
[55] A. Baran, K. Pomorski, A. Łukasiak, and A. Sobiczewski, Nucl. Phys. A **361**, 83 (1981).
[56] J.W. Negele, Nucl. Phys. A **502**, 371c (1989).
[57] J. Skalski, Phys. Rev. C **77**, 064610 (2008).